Exploring Caffeine–Phenol Interactions by the Inseparable Duet of Experimental and Theoretical Data

Imanol Usabiaga
Ander Camiruaga
Camilla Calabrese
Assimo Maris
José A. Fernández

Intermolecular interactions are difficult to model, especially in systems formed by multiple interactions. Such is the case of caffeine–phenol. Structural data has been extracted by using mass-resolved excitation spectroscopy and double resonance techniques. Then the predictions of seven different computational methods have been explored to discover structural and energetic discrepancies between them that may even result in different assignments of the system. The results presented herein highlight the difficulty of constructing functionals to model systems with several competing interactions, and raise awareness of problems with assignments of complex systems with limited experimental information that rely exclusively on energetic data.

INTRODUCTION

Computational chemistry has experienced an impressive evolution, thanks, in part, to the introduction of new computational approaches that can process systems of increasing complexity with a marginal loss of accuracy.[1] One of the most successful approaches has been the introduction of the DFT,[2] as an alternative for other (costly) ab initio approaches, such as Møller–Plesset perturbation theory.[3] The reduced computational cost of DFT methods has enabled very large systems to be tackled, offering an accurate structural and energetic description. Their main drawback is an implicit difficulty in modeling noncovalent interactions that contain a substantial dispersion contribution.[4–6] Still, there is intense ongoing work to optimize the functionals, fitting their parameters to ever-increasing collections of well-known molecular structures. As a result, the number of available functionals is growing fast.[7]

Our group is engaged in the study of noncovalent interactions by using a combined experimental–computational approach.[8, 9] We use mass-resolved excitation spectroscopic techniques to extract structural information about molecular aggregates formed in jets and then we run computations to interpret the experimental data. From that comparison, it is usually possible to determine the number of conformational isomers of the systems and elucidate their structure.[10–12] However, there are difficult cases, such as those in which experimental data are noisy and multiple conformational isomers exist, in which assignment requires of an accuracy in the theoretical prediction that it is not easy to achieve.[13–22] Sometimes, even with excellent experimental data, the systems are so complex that one has to rely on the relative stability of the predicted structures to reach a final assignment. However, accurate prediction of the relative stability of systems containing multiple isomers is not simple, and different functionals may lead to different conclusions. Herein, we explore this issue for a particularly difficult problem: the caffeine–phenol (Caf+Ph) complex. Caffeine (Scheme 1) is a methylxanthine present in coffee and responsible for its stimulant effects.[23] Its structure contains four nitrogen atoms, two oxygen atoms, and an aromatic system, and therefore, exhibits multiple interaction sites for

other molecules. Conversely, phenol is a simple molecule, formed by a benzene ring with a hydroxyl substituent. It is
known to be one of the components of tobacco smoke,[24] and therefore, both molecules may come into contact in the blood of coffee-drinking smokers, and their aggregation may even alter the way in which they interact with different receptors in the cells.[25–28] However, the main goal of this work is not to explore such health-related issues, but to use the spectroscopic information recorded from the aggregates to explore the ability of several computational levels to model the interactions by analyzing the coherence/incoherence of their predictions. This comparison will help us to understand where there are limits for the interpretation of theoretical predictions.

Phenol is prone to form hydrogen bonds with other molecules and it may find six interaction sites in caffeine. The stability of these interactions will also be modulated by C@H···p interactions between the methyl groups and the aromatic ring of phenol and by p···p interactions between the two aromatic rings, leading to a large number of conformational isomers that are very close in stability. Following our usual methodology, we used mass-resolved IR/UV spectroscopy to record the IR spectra and to obtain structural information that we then compared with the results predicted by four different methods: M06-2X, MN15, B3LYP-D3, and MP2. Similar to many other research groups, we have used M06-2X in multiple studies and obtained satisfactory results.[29, 30] However, evidence has appeared lately that has led to questioning of the performance of this functional, in the absence of a leading interaction, such as a strong hydrogen bond.[31–33] Thus, we compared the results of that functional with those of the newest version from the same group: the hybrid MN15. Thrular's group have devoted a significant amount of work to the optimization of their functionals by using the NC87 database.[34, 35]

The third functional, B3LYP corrected by empirical dispersion (ED=GD3BJ),[36] belongs to a completely different family and was reported to yield outstanding results for systems containing noncovalent interactions.[37–40] Certainly, it has become very popular among microwave spectroscopists because it is proven to yield accurate predictions on the structure of stable molecules.[41] As shown below, although all computational levels agreed in the prediction of the most stable structure, a large dispersion was observed for the relative stability of the local minima; this complicates the assignment and highlights the difficulty of modeling systems formed by noncovalent interactions.

RESULTS AND DISCUSSION

Spectroscopy of Caf+Ph

Both phenol and caffeine present discrete absorptions in UV spectroscopy and their spectra have already been reported.[42–45] The spectroscopy of phenol is particularly well known because it is the paradigm of aromatic alcohols.[46–62] Owing to the presence of two chromophores, an excited-state short lifetime, or multiple conformational isomers of the cluster with numerous low-frequency vibrations, the resonance-enhanced multiphoton ionization (REMPI) spectrum of Caf+Ph is a structureless absorption starting at about 35200 cm^{-1} (Figure S1 in the Supporting Information). Similar REMPI spectra were found for other related systems. For example, in a pioneering study, de Vries and co-workers reported the one-color REMPI spectra of 7-methylxanthine and theobromine homodimers and, in both cases, the result was a broad absorption, similar to that

reported herein for caffeine.[42]

The absence of a discrete spectrum precluded the use of isomer-specific spectroscopic techniques, such as UV/UV hole burning. However, it is still possible to estimate the number of isomers that contribute to the REMPI trace by recording the IR/UV spectrum to probe different wavelengths with a UV laser. Figure 1 shows the experimental IR/UV spectra in the OH/CH stretching region, which were obtained for phenol, caffeine, and the Caf+Ph complex, with the probe laser tuned at 36015 and 36 290 cm^{-1}. The IR spectrum of phenol agrees well with previous publications:[63] the single OH stretching band appears as a strong absorption at 3662 cm^{-1}, which means a shift of about 200 cm^{-1} in the complex, and therefore, it is midway between the observed shifts in phenol–water and phenol–ammonia.[64] The group of bands centered at around 3062 cm^{-1} correspond to the CH stretches and are weaker, but still clearly visible in the spectrum. On the other hand, only CH stretches are visible in this region of the IR spectrum of caffeine, and they appear as a single, broad absorption at 2960 cm^{-1}. The IR spectra of the monomers were used to adjust the corrections factors to account for anharmonicity in computed frequencies. As observed in Figure 1, all seven computational levels produced very similar predictions, and accurately reproduced the experimental observations. However, the anharmonicity factors required to correct the band positions were significantly different for each computational level. Interestingly, a more similar factor for both CH and OH stretches was required for computations with def2tzvp and a single value for both types of stretches was required at the B3LYPED= GD3BJ/def2tzpv level.

As observed in Figure 1, the two IR spectra of Caf+Ph obtained upon probing two different wavelengths are noisy, but still they present small but noticeable differences; thus indicating population changes with the UV wavelength and providing evidence of the contribution of several isomers to the spectrum. Furthermore, only the OH stretch is expected to appear in that spectral region, while the broad absorption presents a shoulder, which may be due to the existence of additional isomers or to fragmentation from larger clusters. However, the weak signal of the dimer and the absence of signals in the mass spectrum that could be attributed to the trimer exclude such a possibility. The other possible fragmentation source is water complexes, but in this experimental arrangement the formation of water complexes is so disfavored that even phenol+water or caffeine+water complexes are hard to detect.

Assignment of the IR spectrum requires a comparison with the computational predictions, but the shift in the OH stretch of phenol clearly indicates that the participant molecules form a moderately strong hydrogen bond.

Exploration of the conformational landscape revealed the existence of several possible isomers for phenol interacting with each interaction site of caffeine. The differences between them are due to the secondary interactions, which are maximized in each case. For example, as shown in Figure 2, if phenol interacts with OC_6, it can also interact with the aromatic ring (isomers 1 and 6) or with one of the methyl groups (isomer 7, 17), or just maximize the O@H···O interaction, by positioning the phenolic ring away from caffeine (isomer 12, see also Figures S2–S5 in the Supporting Information). It is very likely that many of the computed structures are connected by low potential-energy barriers, and therefore, the whole system simplifies during the cooling process, leading to a reduced

number of structures in the expansion. Thus, information on the relative stability of the computed structures may be helpful for the assignment of experimental spectra.

Figure 3 shows the binding Gibbs free energy (DDG) of the structures calculated at the seven levels. All theoretical approaches point to isomer 1 as the most stable structure at 0 K followed by isomer 2. However, some discrepancies in the relative energetic order of the rest of the structures were found: the standard deviation (SD) of DDG between the seven computational methods (labeled as BM; Figure 3) is larger than the SD of DDG between conformers (labeled as BC), which means that the energy difference between most of the conformers is within the computational error. All of these error estimations were performed without considering the structures with a RMSD in the atomic positions of >0.4, since, for those conformers, the optimization step resulted in very different structures. Surprisingly, the same trends were observed for calculations with MP2, regarding dispersion of the computed values and it presented one of the highest SDs. Optimization with MP2 also resulted in a reduced number of isomers because some of the conformers found by the other calculation levels converged in a single structure under MP2 calculations (see Table S1 in the Supporting Information). The discrepancies are maximized at higher temperatures. For example, at 298 K, the ratio between BM and BC SDs is inverted, which means that the computational error is larger than the energy difference between conformers. Therefore, it is more convenient to consider only families of structures and trends instead of isolated conformations. Other evidence of this fact can be found in Figure S6 in the Supporting Information, in which the Gibbs free energy diagrams for the seven theory levels are presented. In the diagrams, it is clear that at low temperature isomer 01 is the most stable conformers for all computational levels, closely followed by isomer 02. However, at 298 K, there are stability inversions between members of the same family and even between families of structures. However, the most stable families always present a strong OH$\cdots$OC interaction (dotted lines in Figure 3). The isomers that present such interactions are 10, 11, 16, and 15 for the OH$\cdots$OC$_2$ interaction and isomers 07, 12, and 17 for the OH$\cdots$OC$_6$ interaction. Inside this latter family, conformer 06$_{-07}$ was a stable structure for B3LYP and corresponded to a structure midway between that of isomers 06 and 07, although the intermolecular interaction fitted better with those in isomer 07.

All of the above highlights that, in general, the relative stability may only be used to assign (at most) the spectrum of the most stable isomer, if the temperature of the beam is close to 0 K. Above a certain temperature, a comparison with experimental data becomes essential, especially if attractive forces are composed of several weak interactions or several conformers are found in a narrow stability window.

Regarding the computed normal modes, once more, important discrepancies were found between the computation methods. Figure 4 shows a comparison between the DFT predictions and the experimental traces. The predictions are grouped with respect to the type of interaction that keeps the two moieties together by using the same color patterns as those in Figures 2 and 3. For example, those isomers with the OH$\cdot$OC$_6$ interaction are shaded in red (Caf+Ph 01, 06) or dark red (Caf+Ph 07, 12, and 17).

The comparison between experiment and predictions shown in Figure 4 does not offer a univocal assignment. Clearly, those structures in which phenol is interacting with N$_9$ can be discarded because they present absorptions that are either

to the blue (Caf+Ph 03, 04, and 05) or to the red (depicted in dark blue, Caf+Ph 13) of the experimental observations. Likewise, the predictions for isomer 8 (orange) do not match the experimental spectrum. However, isomer 14 may reproduce the position of the shoulder at all levels apart from the two M06-2X computational levels. This also correlates with the large RMSD deviation due to a large structural change during optimization at the M06-2X level. Such structural changes also occur in other conformers, such as Caf+Ph 06, 08, 16, and 17, resulting in very different predicted IR spectra. The computed spectra for the rest of the species and families present transitions that are compatible with the experimental spectra. A more accurate assignment would also need to take into account, in addition to the relative stability of the structures, the shape of the potential-energy surface. However, the differences in the values offered by each computational level do not clarify which of the methods would yield the most accurate description of the conformational space, especially at 298 K. Notably, those families that become more stable at this temperature are those that better reproduce the position of the strong absorption in the spectra (dark red and dark green in Figure 5).

In summary, in Figure 5, we compare the position of the OH stretch predicted for the most stable families with the experimental spectrum. The width of the bars represents the uncertainty in the position of the transition. Clearly, the whole experimental trace is explained by the transitions predicted for these families: the maximum of the absorption correlates very well with the OH stretching of those families that are stable at higher temperatures and present a strong OH·$OC_{2,6}$ hydrogen bond. Likewise, the shoulder is well reproduced by the structures that are more stable at 0 K and that present stacking interactions in addition to the OH·$OC_{2,6}$ hydrogen bond.

In any case, the panorama depicted herein is worrisome: all four functionals seem to be well designed to describe the strong interactions that form the most stable isomers. However, the differences in their coefficients to describe weaker interactions result in fuzzy predictions of the local minima. This problem is maximized at 298 K and presumably at the temperature of living beings. Furthermore, the discrepancies observed in a small system, such as Caf+Ph, may be amplified if dealing with larger systems, such as protein folding or protein–ligand aggregates, in which the interactions due to dispersive forces play a determining role in the final shape of the system.

CONCLUSION

We presented a combined computational and experimental examination of Caf+Ph aggregates. Despite the relatively small size of the system, it proved to be a complex problem: caffeine presents several interaction sites for phenol, with numerous local minima, resulting from the balance between C@H···p and p···p interactions. Furthermore, the experimental observations were limited to the shift in the OH stretching band, as a result of intermolecular interactions.

Seven different computational levels were used to describe the system and to assign the experimental spectra: M06-2X, MN15, and B3LYP-ED=GD3BJ combined each one with the bases 6-311++G(d,p), def2tzpv, and MP2/6-311++G(d,p). All seven agreed that conformer 1 is the most stable structure and isomer 2 is the second one. In such conformers, phenol interacts with caffeine through p···p interactions and a hydrogen bond with C=O of caffeine. This assignment would be in

agreement with previous studies on caffeine–water, in which water was also found to interact preferentially with the carbonyl groups of caffeine.[44, 45, 65] However, no consensus was found between them for the relative stability of the local minima. This seems to indicate that the methods used are able to accurately model stronger interactions, but they balance other weaker interactions in different ways. The magnitude of the discrepancies between the predictions is assumed to be due to differences in the strengths of the secondary interactions, and therefore, in the low-frequency modes.

The panorama resulting from this work warns about overinterpreting the results of these kinds of studies. The complexity of the system, limited amount of experimental information, and implicit precision of the computations limit the conclusions that one can extract. We can affirm that phenol preferentially interacts with OC_6 and that the most likely secondary interaction site is OC_2. Such interactions result in a broad absorption centered at around 3450 cm@1. Other isomers may also contribute to the spectrum, with the interaction with the same oxygen atoms as a leading force, but with a different ratio of contributions of other secondary interactions (mainly stacking and CH···p). Determining the structure of the system more pre- cisely would require additional experimental and computation data.

EXPERIMENTAL SECTION

Experimental details
The experimental details were described in previous works.[30] The setup was composed of a supersonic expansion chamber equipped with a laser ablation system. This device allowed us to vaporize thermolabile molecules. The chamber was coupled with a TOF mass spectrometer, to carry out mass-selected detection. For the ionization of the supersonically expanded samples, a UV laser (Quantel Qscan) was used and an IR-OPO laser (LaserVision) was added for the double resonance experiments.

The supersonic expansion worked with 10 bar of backing pressure of argon (Praxair, 2X, 99.998% purity). Sample preparation required careful optimization. Phenol, with a melting point of 313 K, produces an entropy increase upon mixing with carbon nanotubes and/ or caffeine that was sufficient to induce its melting. Finally, the following protocol was adopted: first, a mixture of caffeine and carbon nanotubes (&60:40 v/v) was produced and deposited on the surface of a rod-shaped sample holder. Then, a solution of phenol in diethyl ether was sprayed over the surface of the sample. Ablation of the mixture created synchronously with the aperture of the pulsed valve resulted in the creation of a jet seeded with caffeine and phenol, which, under the cooling conditions of the expansion, aggregated to form clusters. Nevertheless, the concentration of caffeine and phenol in the beam was low, which produced a weak signal and hampered the formation of larger clusters. No signal from phenol/water or caffeine/water clusters was detected.

Computational details
The computational procedure started with a conformational search, which was carried out by using three different force fields: MMFFs,[66] AMBER,[67] and OPLS 2005.[68] The redundant conformations were identified by clustering of all structures. The identified candidates were optimized with M06-2X/6-311++G(d,p) and further confirmed as true minima in a normal mode analysis. After the exclusion of redundant conformations, the remaining structures were optimized at the level of each of the other methods: M06-2X/ def2tzpv, MN15, and B3LYP-ED=GD3BJ with 6-311++

G(d,p), def2tzpv, MP2/6-311++G(d,p), and MP2/6-311++G(d,p).
Theoretical simulations of the IR spectrum were generated by applying
a correction factor to the normal modes obtained from the
Gaussian program package.[69] The factors were empirically determined
by fitting the simulations to the experimental frequencies
of the monomers (see Figure 1). The resulting lines were represented
by using a Lorentzian function, with a variable width, depending
on the region of the spectrum and the type of interaction.
Stronger hydrogen-bond interactions were assumed to produce
broader absorptions, shifted to the red. The effect of the laser on
the shape of the transition was also taken into account by the convolution
of a Gaussian function with the Lorentzian simulation.

ACKNOWLEDGEMENTS

## REFERENCES

[1] V. Barone, R. Improta, N. Rega, Acc. Chem. Res. 2008, 41, 605–616.
[2] A. D. Becke, J. Chem. Phys. 1993, 98, 5648–5652.
[3] C. Møller, M. S. Plesset, Phys. Rev. 1934, 46, 618–622.
[4] E. R. Johnson, I. D. Mackie, G. A. DiLabio, J. Phys. Org. Chem. 2009, 22,
1127–1135.
[5] P. Jurecˇka, J. Cˇerny´, P. Hobza, D. R. Salahub, J. Comput. Chem. 2007, 28,
555–569.
[6] R. Podeszwa, K. Szalewicz, J. Chem. Phys. 2012, 136, 161102.
[7] J. F. Dobson, K. Burke, J. P. Perdew, Electronic Density Functional Theory
Recent Progress and New Directions, Springer US, 1998.
[8] I. Lejn, J. Mill#n, E. J. Cocinero, A. Lesarri, J. A. Fern#ndez, Angew. Chem.
Int. Ed. 2013, 52, 7772–7775; Angew. Chem. 2013, 125, 7926–7929.
[9] I. Lejn, I. Usabiaga, P. F. Arnaiz, A. Lesarri, J. A. Fern#ndez, Chem. Eur. J.
2018, 24, 10291–10295.
[10] P. S. Walsh, K. N. Blodgett, C. McBurney, S. H. Gellman, T. S. Zwier,
Angew. Chem. Int. Ed. 2016, 55, 14618–14622; Angew. Chem. 2016, 128,
14838–14842.
[11] M. Alauddin, E. Gloaguen, V. Brenner, B. Tardivel, M. Mons, A. Zehnacker-
Rentien, V. Declerck, D. J. Aitken, Chem. Eur. J. 2015, 21, 16479 –
16493.
[12] I. Usabiaga, J. Gonz#lez, I. Lejn, P. F. Arnaiz, E. J. Cocinero, J. A. Fern#ndez,
J. Phys. Chem. Lett. 2017, 8, 1147–1151.
[13] C. C8zard, C. A. Rice, M. A. Suhm, J. Phys. Chem. A 2006, 110, 9839 –
9848.
[14] M. Nedic´, T. N. Wassermann, R. W. Larsen, M. A. Suhm, Phys. Chem.
Chem. Phys. 2011, 13, 14050–14063.
[15] C. Pletzer, I. Henig, K. Kleinermanns, E. Nir, M. S. de Vries, ChemPhys-
Chem 2003, 4, 838–842.
[16] N. Borho, M. A. Suhm, Phys. Chem. Chem. Phys. 2002, 4, 2721–2732.
[17] R. N. Casaes, J. B. Paul, R. P. McLaughlin, R. J. Saykally, T. van Mourik, J.
Phys. Chem. A 2004, 108, 10989–10996.
[18] G. M. Florio, T. S. Zwier, J. Phys. Chem. A 2003, 107, 974–983.
[19] D. Zimmermann, T. H. H-ber, H. Schaal, M. A. Suhm, Mol. Phys. 2001, 99,
413–425.
[20] F. Piuzzi, I. Dimicoli, M. Mons, P. Milli8, V. Brenner, Q. Zhao, B. Soep, A.
Tramer, Chem. Phys. 2002, 275, 123–147.
[21] T. S. Zwier, J. Phys. Chem. A 2001, 105, 8827–8839.
[22] I. Dauster, C. A. Rice, P. Zielke, M. A. Suhm, Phys. Chem. Chem. Phys.
2008, 10, 2827–2835.
[23] A. Nehlig, J. L. Daval, G. Debry, Brain Res. Rev. 1992, 17, 139–170.
[24] A. Rodgman, T. Perfetti, The Chemical Components of Tobacco and Tobacco

Smoke, CRC, Boca Raton, 2013.

[25] T. T. Lang, J. D. Young, C. E. Cass, Mol. Pharmacol. 2004, 65, 925–933.
[26] B. B. Fredholm, K. B-ttig, J. Holm8n, A. Nehlig, E. E. Zvartau, Pharmacol. Rev. 1999, 51, 83–133.
[27] S. Zevin, N. L. Benowitz, Clin. Pharmacokinet. 1999, 36, 425–438.
[28] J. Istvan, J. D. Matarazzo, Psychol. Bull. 1984, 95, 301–326.
[29] I. Usabiaga, J. Gonz#lez, P. F. Arn#iz, I. Lejn, E. J. Cocinero, J. A. Fern#ndez, Phys. Chem. Chem. Phys. 2016, 18, 12457–12465.
[30] A. Camiruaga, I. Usabiaga, A. Insausti, I. Lejn, J. A. Fern#ndez, Phys. Chem. Chem. Phys. 2017, 19, 12013–12021.
[31] M. Juanes, W. Li, L. Spada, L. Evangelisti, A. Lesarri, W. Caminati, Phys. Chem. Chem. Phys. 2019, 21, 3676–3682.
[32] I. lejn, R. Montero, A. Longarte, J. Fern#ndez, J. Chem. Phys. 2013, 139, 174312.
[33] C. P8rez, I. Lejn, A. Lesarri, B. H. Pate, R. Mart&nez, J. Mill#n, J. A. Fern#ndez, Angew. Chem. Int. Ed. 2018, 57, 15112–15116; Angew. Chem. 2018, 130, 15332–15336.
[34] H. S. Yu, X. He, D. G. Truhlar, J. Chem. Theory Comput. 2016, 12, 1280 – 1293.
[35] H. S. Yu, X. He, S. L. Li, D. G. Truhlar, Chem. Sci. 2016, 7, 5032–5051.
[36] S. Grimme, J. Antony, S. Ehrlich, H. Krieg, J. Chem. Phys. 2010, 132, 154104.
[37] E. Caldeweyher, C. Bannwarth, S. Grimme, J. Chem. Phys. 2017, 147, 034112.
[38] S. Grimme, S. Ehrlich, L. Goerigk, J. Comput. Chem. 2011, 32, 1456 – 1465.
[39] S. Grimme, J. Comput. Chem. 2006, 27, 1787–1799.
[40] S. Grimme, J. Comput. Chem. 2004, 25, 1463–1473.
[41] I. Uriarte, A. Insausti, E. J. Cocinero, A. Jabri, I. Kleiner, H. Mouhib, I. Alkorta, J. Phys. Chem. Lett. 2018, 9, 5906–5914.
[42] M. P. Callahan, Z. Gengeliczki, N. Svadlenak, H. Valdes, P. Hobza, M. S. de Vries, Phys. Chem. Chem. Phys. 2008, 10, 2819–2826.
[43] A. Oikawa, H. Abe, N. Mikami, M. Ito, J. Phys. Chem. 1983, 87, 5083 – 5090.
[44] D. Kim, H. M. Kim, K. Y. Yang, S. K. Kim, N. J. Kim, J. Chem. Phys. 2008, 128, 134310.
[45] P. B. Balbuena, W. Blocker, R. M. Dudek, F. A. Cabrales-Navarro, P. Hirunsit, J. Phys. Chem. A 2008, 112, 10210–10219.
[46] H. Watanabe, S. Iwata, J. Chem. Phys. 1996, 105, 420–431.
[47] K. Fuke, K. Kaya, Chem. Phys. Lett. 1983, 94, 97–101.
[48] R. J. Stanley, A. W. Castleman, J. Chem. Phys. 1991, 94, 7744–7756.
[49] D. Solgadi, C. Jouvet, A. Tramer, J. Phys. Chem. 1988, 92, 3313–3315.
[50] C. Jouvet, C. Lardeux-Dedonder, M. Richard-Viard, D. Solgadi, A. Tramer, J. Phys. Chem. 1990, 94, 5041–5048.
[51] J. Steadman, J. A. Syage, J. Chem. Phys. 1990, 92, 4630–4632.
[52] J. A. Syage, J. Steadman, J. Chem. Phys. 1991, 95, 2497–2510.
[53] J. A. Syage, Faraday Discuss. 1994, 97, 401–413.
[54] M. F. Hineman, D. F. Kelley, E. R. Bernstein, J. Chem. Phys. 1993, 99, 4533–4538.
[55] R. J. Lipert, S. D. Colson, Chem. Phys. Lett. 1989, 161, 303–307.
[56] R. J. Lipert, G. Bermudez, S. D. Colson, J. Phys. Chem. 1988, 92, 3801 – 3805.
[57] T. Ebata, N. Mizuochi, T. Watanabe, N. Mikami, J. Phys. Chem. 1996, 100, 546–550.
[58] M. Schmitt, H. Meller, K. Kleinermanns, Chem. Phys. Lett. 1994, 218, 246–248.
[59] S. Tanabe, T. Ebata, M. Fujii, N. Mikami, Chem. Phys. Lett. 1993, 215, 347–352.
[60] T. Watanabe, T. Ebata, S. Tanabe, N. Mikami, J. Chem. Phys. 1996, 105, 408–419.
[61] K. Kleinermanns, S. Schumm, W. Perl, U. Henrichs, M. Gerhards, C. Jacoby, J. Chem. Phys. 2002, 104, 9362–9375.
[62] T. Bergi, M. Schetz, S. Leutwyler, J. Chem. Phys. 1995, 103, 6350–6361.
[63] E. Aguado, I. Lejn, E. J. Cocinero, A. Lesarri, J. A. Fern#ndez, F. CastaÇo, Phys. Chem. Chem. Phys. 2009, 11, 11608–11616.
[64] A. Iwasaki, A. Fujii, T. Watanabe, T. Ebata, N. Mikami, J. Phys. Chem. 1996, 100, 16053–16057.
[65] V. B. Singh, RSC Adv. 2014, 4, 58116–58126.
[66] T. A. Halgren, J. Comput. Chem. 1996, 17, 490–519.
[67] D. A. Case, T. E. Cheatham, T. Darden, H. Gohlke, R. Luo, K. M. Merz, A. Onufriev, C. Simmerling, B. Wang, R. J. Woods, J. Comput. Chem. 2005, 26, 1668–1688.
[68] M. J. Robertson, J. Tirado-Rives, W. L. Jorgensen, J. Chem. Theory Comput. 2015, 11, 3499–3509.
[69] Gaussian 16, Revision D0.1, M. J. Frisch, G. W. Trucks, H. B. Schlegel, G. E. Scuseria, M. A. Robb, J. R. Cheeseman, G. Scalmani, V. Barone, G. A. Petersson,

H. Nakatsuji, X. Li, M. Caricato, A. V. Marenich, J. Bloino, B. G. Janesko, R. Gomperts, B. Mennucci, H. P. Hratchian, J. V. Ortiz, A. F. Izmaylov, J. L. Sonnenberg, D. Williams-Young, F. Ding, F. Lipparini, F. Egidi, J. Goings, B. Peng, A. Petrone, T. Henderson, D. Ranasinghe, V. G. Zakrzewski, J. Gao, N. Rega, G. Zheng, W. Liang, M. Hada, M. Ehara, K. Toyota, R. Fukuda, J. Hasegawa, M. Ishida, T. Nakajima, Y. Honda, O. Kitao, H. Nakai, T. Vreven, K. Throssell, J. A. Montgomery, Jr., J. E. Peralta, F. Ogliaro, M. J. Bearpark, J. J. Heyd, E. N. Brothers, K. N. Kudin, V. N. Staroverov, T. A. Keith, R. Kobayashi, J. Normand, K. Raghavachari, A. P. Rendell, J. C. Burant, S. S. Iyengar, J. Tomasi, M. Cossi, J. M. Millam, M. Klene, C. Adamo, R. Cammi, J. W. Ochterski, R. L. Martin, K. Morokuma, O. Farkas, J. B. Foresman, D. J. Fox, Gaussian, Inc., Wallingford CT 2016.
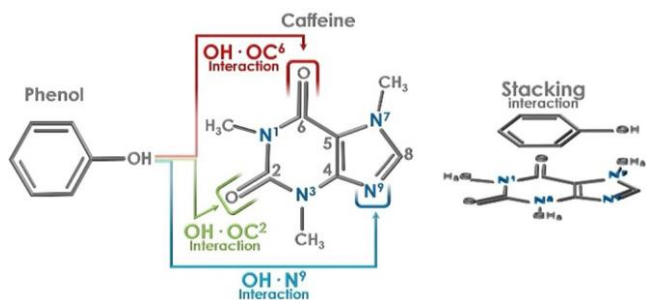
Scheme 1. Structure of phenol and caffeine (with atom numbering). The four main interacting sites, OH·OC_6, OH·OC_2, OH·N_9, and the stacking interaction, are highlighted.
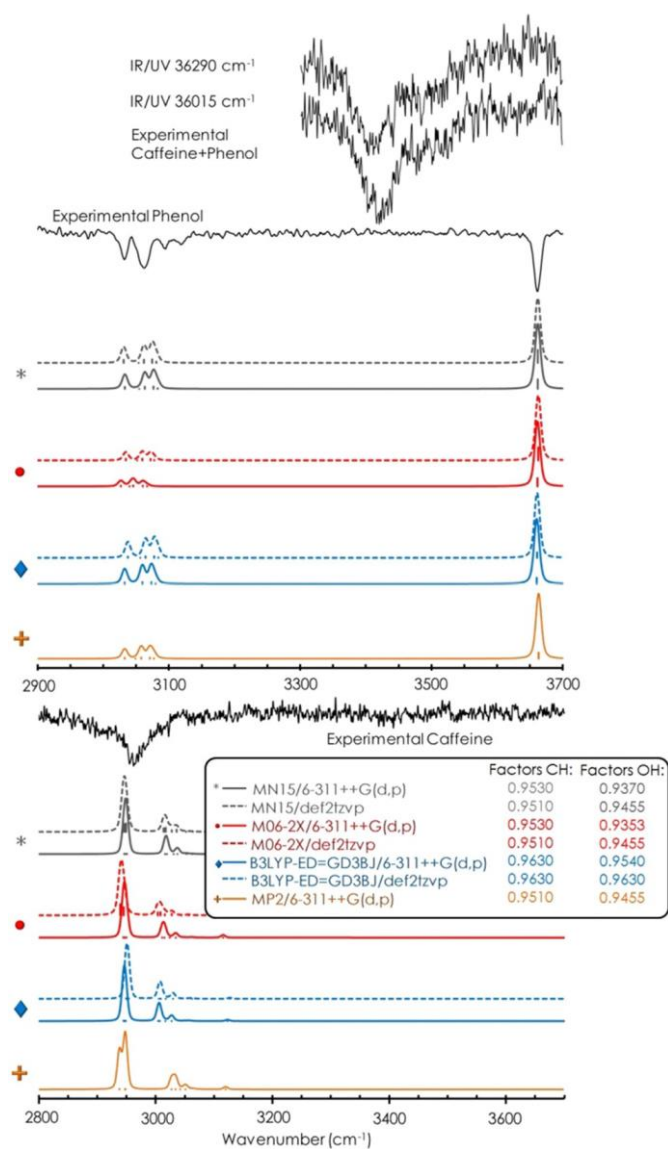
Figure 1. IR/UV spectra of caffeine, phenol, and Caf+Ph. A comparison of the spectra of caffeine and phenol with computational predictions allowed us to determine the value of the factors that account for anharmonicity at each computational level. Interestingly, a single factor for both CH and OH stretches was required at the B3LYP-ED=GD3BJ/def2tzvp level.
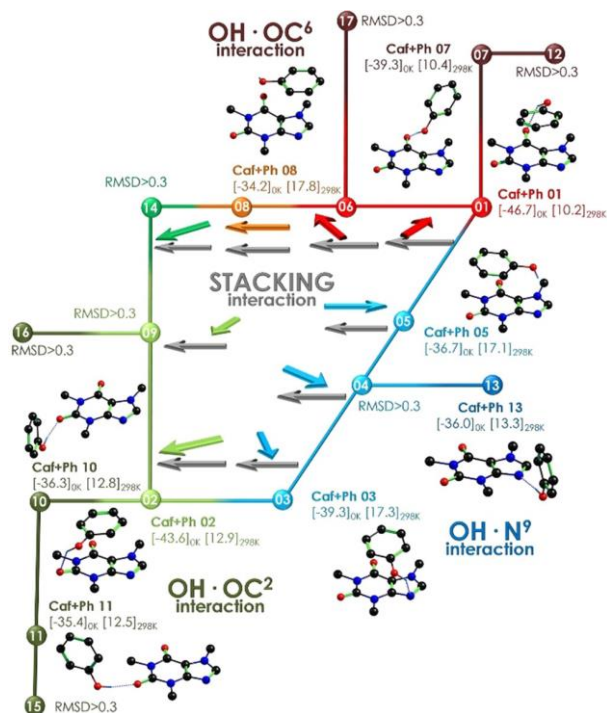

Figure 2. Computed structures of Caf+Ph, which are sorted according to similarity and interaction site. Binding Gibbs free energy values DDG [kJmol$_{@1}$] are given at 0 and 298 K, and they are the average of the six theoretical methods, considering only structures with a root-mean-square deviation (RMSD) of atomic positions (counting only C and O atoms) of <0.3. MP2 was not included because several of the structures predicted by the other methods converged to the same conformer upon optimization at MP2. The arrows depict the relative orientation of the two molecules in stacking. All hydrogen atoms attached to a carbon atom were hidden for the sake of clarity. More elaborate versions of this figure, with the relative stability of the structures calculated at each computational level, can be found in Figures S2–S5 in the Supporting Information.
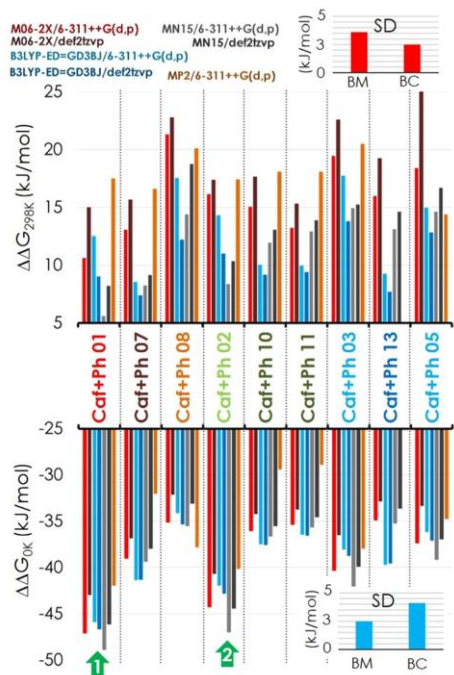
Figure 3. Relative binding Gibbs free energy (DDG) diagram at 0 and 298 K for the conformers of Caf+Ph with RMSD of atomic positions of <0.3. See also Figure S6 and Table S1 in the Supporting Information. DDG is defined as the difference in DG of a given species with the global minimum. SD=standard deviation, BM=between methods, BC=between conformers
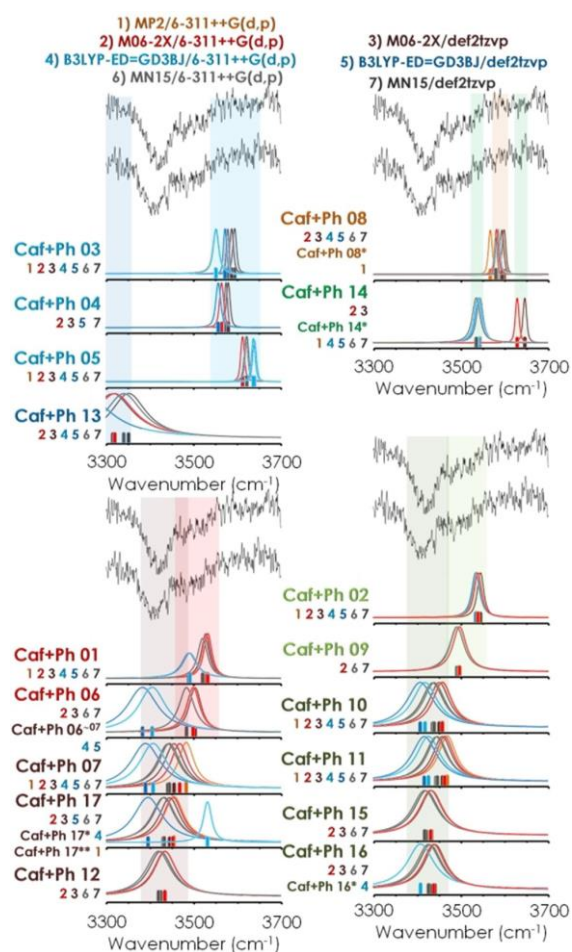
Figure 4. A comparison between the IR spectra of Caf+Ph and the computational predictions for the calculated structures. The structures are grouped by the type of interaction. The position of the bands is simulated by using gaussians that follow the color code of the computational level.
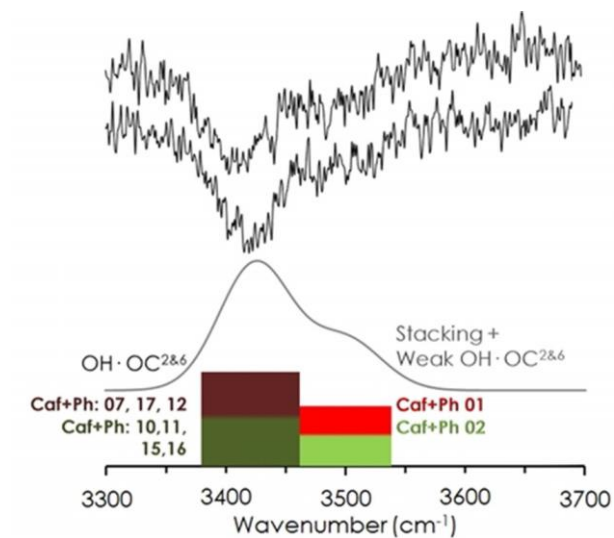

Figure 5. A comparison between the prediction of the position of the OH stretch for the four main families of isomers and the experimental spectrum. The width of the bars indicates the uncertainty in the prediction of the band position. A simulation with two gaussians is also offered (gray curve).